Accepted Manuscript

This is an *Accepted Manuscript*, which has been through the RSC Publishing peer review process and has been accepted for publication.

Accepted Manuscripts are published online shortly after acceptance, which is prior to technical editing, formatting and proof reading. This free service from RSC Publishing allows authors to make their results available to the community, in citable form, before publication of the edited article. This *Accepted Manuscript* will be replaced by the edited and formatted *Advance Article* as soon as this is available.

To cite this manuscript please use its permanent Digital Object Identifier (DOI®), which is identical for all formats of publication.

More information about *Accepted Manuscripts* can be found in the **Information for Authors**.

Please note that technical editing may introduce minor changes to the text and/or graphics contained in the manuscript submitted by the author(s) which may alter content, and that the standard **Terms & Conditions** and the **ethical guidelines** that apply to the journal are still applicable. In no event shall the RSC be held responsible for any errors or omissions in these *Accepted Manuscript* manuscripts or any consequences arising from the use of any information contained in them.

Journal Name

Dynamic Article Links ▶

ARTICLE TYPE

Panchromatic Porous Specular Back Reflectors for Efficient Transparent Dye Solar Cells

Carmen López-López, Silvia Colodrero, Hernán Míguez*

A panchromatic specular reflector based dye solar cell is herein presented. Photovoltaic performance of this novel design is compared to that of cells in which standard diffuse scattering layers are integrated. The capability of the proposed multilayer structures to both emulate the broad band reflection of diffuse scattering layers of standard thickness (around 5 microns) and give rise to similarly high light harvesting and power conversion efficiencies, yet preserving the transparency of the device, is demonstrated. Such
10 white light reflectors are comprised of stacks of different porous optical multilayers, each one displaying a strong reflection at a complementary spectral range, and are designed to leave transmittance unaltered in a narrow red-frequency range at which the sensitized electrode shows negligible absorption, thus allowing to see through the cell. The reflectance bandwidth achieved is three times as broad as the largest
15 previously achieved with any photonic structure integrated in a dye solar cell.

Introduction

The use of back diffuse scattering layers has become a standard technique to largely increase light harvesting efficiency in the field of dye solar cells (DSC).[1-5] This improvement occurs at the
20 expense of bringing to an end one of its main added values for building integrated photovoltaics: its transparency. Alternative optical designs based on photonic nanostructures that could overcome this drawback have been proposed, [6-12] but so far none of them have shown efficiency enhancements comparable to
25 those attained with a packing of disordered submicrometric particles. In fact, previous attempts by our group and coworkers to achieve this goal based on the substitution of the diffuse scattering layer by a porous one dimensional photonic crystal led to improved cells that perform as good as those integrating
30 diffuse scattering layers of similar thickness (<2 micron),[7] but not as much as a standard 5 micron thick diffuse scattering layer (DSL). This difference could be overcome by creating dielectric mirrors of higher reflectance on broader spectral bands, which implies increasing the number of unit cells, so they can be as
35 efficient as DSL. However, enlarging thickness of the originally proposed multilayer structures yielded strongly hindered electrolyte diffusion, which resulted in an abrupt decrease of all relevant photovoltaic parameters (photocurrent, photovoltage, fill factor) for mirrors above 4 unit cells (please see figure S1).
40 Recently, it was demonstrated that addition of porogens to the constituent layers allowed achieving optical quality films with large overall porosity and wide pore size distribution,[13] which resulted in improved electrolyte diffusion through thick multilayers with minimum impact on fill factor and photovoltage.
45 Such advance permitted to create DSC devices that combine

tuneable colour and semitransparency with efficient energy conversion.[10,12]

In this communication, we present a panchromatic porous dielectric mirror that, when integrated in a DSC, yields
50 photocurrent and efficiency enhancements comparable to those attained with diffuse scattering layers of standard thickness, yet preserving transparency. This is accomplished by devising a layered structure containing multiple periodicities that, when interacting with incoming light, provide a broad spectral band
55 reflection only in the wavelength range at which the dye effectively absorbs, leaving transmittance unaltered in a narrow red-frequency range at which absorption is negligible.

Experimental section

Preparation of TiO$_2$ electrodes.

60 Before the deposition of the TiO2 layer, the FTO glass substrates (TEC 11Ω/cm2, Nippon Sheet Glass) were soaked in 0.04 M TiCl4 aqueous solution at 70 °C for 15 min, washed with distilled water and ethanol and dried at room temperature. After that, a paste containing TiO2 nanoparticles (18-NRT, Dyesol®) was
65 coated onto the FTO by screen printing, resulting active layers with areas of 0.25 cm^2 and thicknesses of 4.5 μm. Subsequently, the films were thermally annealed at 500 ^{0}C under air flow. The sintered electrodes were soaked again into a 0.04 M TiCl4 aqueous solution at 70 °C for 15 min and then washed with water
70 and ethanol, and finally heated at 450 ^{0}C. All electrodes used in this work were carefully selected after checking their thickness and roughness using a motorized profilometer (Mahr®-perthometer PGK), so they could be employed for an appropriate comparison between reference, diffuse scattering layer based
75 cells and specular panchromatic reflector based cells. Thickness

variation with respect to the total thickness of the film was in the range of ±5 % in all cases.

Preparation of specular panchromatic reflectors coupled to TiO_2 electrodes.

First, the optical properties of different designs of structures made of a stack of three mirrors, each one having a different unit cell, were simulated using the same MatLab codes employed in reference [15]. Once the optimized combination of mirrors were found, we proceeded with their fabrication. The starting materials to build each one of the multilayers that form the stack were SiO_2 nanospheres (average size of 30nm) purchased from Dupont (34 wt% suspension in H_2O, LUDOX® TMA), and TiO_2 nanocrystallites in a final concentration of 25 wt% (average size of 6 nm) synthesized as previously reported.[14] To prepare the precursor suspensions to be employed during the deposition process, both types of nanoparticles were suspended in a mixture of water (21% vol) and methanol (79% vol). TiO_2 dispersions also contained a certain amount of polymer (PEG 20000, Fluka) following the weight relation of PEG:TiO_2=0.5, which has been proven to increase the porosity and the pore size distribution of these films.[12] The periodic structure was then fabricated by stacking alternate layers made of such suspensions using a spin coater Laurell WS-400E-6NPP working at final speed of 5000 rpm and an acceleration of 9180 rpms-1. The unit cell thickness variation in the panchromatic reflector structure is achieved by using different TiO_2 concentration in the precursor suspensions employed to build each type of photonic crystal. After each deposition of TiO_2/PEG suspension, a heat treatment (300 ^{0}C 15 min) was used to remove the polymer. Finally, all samples were annealed at 450 ^{0}C for 30 min.

Preparation of a TiO_2 scattering layer based DSC.

A paste containing TiO_2 large particles (WER2-O, Dyesol®) was used to built 4.5 μm scattering layers. This layer was deposited via screen printing on top of the transparent electrodes. Finally, the scattering layers were also subjected to thermal treatment, which was carried out at 450^{0}C during 30min.

Fabrication of DSCs.

The working electrodes were dipped overnight into a 0.2 mM dye solution (N719, Solaronix®) using ethanol as solvent, followed by rinsing in ethanol and dried. Counterelectrodes were made by drop deposition of colloidal platinum paste (Platisol T, Solaronix®) onto a conductive FTO glass substrate and heated at 400 ^{0}C for 10 minutes. The dyed TiO_2 electrodes were assembled with the Pt counter electrode by using a thermo-polymer (Surlyn Meltonix 1170-25, Solaronix) as spacer between them. The electrolyte consisted of 100 mM I2 (Aldrich, 99.999%), 100 mM LiI (Aldrich, 99.9%), 600 mM [(C4H9)4N]I (Aldrich, 98%), and 500mM 4-tert-butylpyridine (Aldrich, 99%) in 3-methoxy propionitrile (Fluka, ≥99%), and was infiltrated into the cell through two holes made previously at the back of the counterelectrode.

Optical and photovoltaic characterization.

Transmittance and total reflectance spectra were performed using an ultraviolet-visible scanning spectrophotometer (SHIMADZU UV-2101PC). IV characterization was carried out with a solar simulator (Sun 2000, Abet Technologies) including a 150 W arc xenon lamp and the appropriate filter to replicate the AM1.5 solar spectrum. IV curves were obtained by applying an external bias to the cell and measuring the generated photocurrent with a digital source meter (Keithley 2400). Incident photon to collected electron (IPCE) efficiency measurements were acquired using a home-built system composed of a 300 W xenon lamp, a monochromator with 1140 lines/mm grating (Model 272, Mcpherson) controlled by a digital scan drive system (Model 789A-3, Mcpherson) and a picoamperemeter (Keithley 6485). An UV filter with cut-off wavelength of 400 nm was used to remove second order harmonics exiting the monochromator. A silicon photodiode with calibration certificate (D8-Si-100 TO-8 Detector, Sphere Optics) was used to correct the cell response. To reduce spureous light reflections and refractions, which might lead to erroneous interpretations, all measurements were performed using a black mask covering the device. Angular measurements were taken using a sample holder attached to a rotating stage, with an angular scale resolution of 10 arc min. 0 degree refers to light incidence normal to the cell surface.

The reproducibility and reliability of all results herein presented were confirmed by realizing nine cells of each type and performing the same structural and photovoltaic characterization for all of them.

Results and Discussion

For the purpose of comparison, two sorts of highly reflecting photonic structures and a diffuse scattering layer are built onto the TiO_2 electrodes. Among the former, one of them is a nanoparticle based one dimensional photonic crystal (1DPC) fabricated by stacking a total of eight porosity enhanced SiO_2-TiO_2 nanoparticle bilayers, in which the TiO_2 and SiO_2 thicknesses (100 and 90 nm respectively) are kept constant throughout the multilayer. The other is a hierarchical structure constructed from three different 1DPCs deposited one on top of each other. Each one of them has a thickness of 4 unit cells (1 unit cell equals 1 TiO_2-SiO_2 bilayer). In this case, the thickness of the SiO_2 layer is fixed for the entire multilayer at 90 nm, while the TiO_2 layer thickness decreases along the direction of incident light from 125 nm in the first Bragg stack to 95 nm and 60 nm in the second and third ones. This configuration allows attaining highly reflecting structures covering almost the whole visible range and hence displaying a strong white reflection (Please see supplementary figure S2), preserving at the same time the electrode transparency for the longest visible wavelengths, as it can be seen in the pictures displayed in figure 1.a. It should be remarked that the same dielectric mirrors inversely arranged, so that the lattice constant increases in the direction of incoming light, would result in a lower reflectance structure even with narrow transmission windows located at highly absorbing spectral ranges of the dye. Please see the simulated reflectance, attained with the same code[15] used to design the panchromatic structure, resulting from placing the mirrors in reverse other in figure S3 and the experimental confirmation of such effect in figure S4. For the sake of comparison, a picture of a cell made of a similar nanocrystalline electrode but coupled to a diffuse scattering layer is shown in figure 1.b. Please notice that the underlying text can only be seen through the cell coupled to the
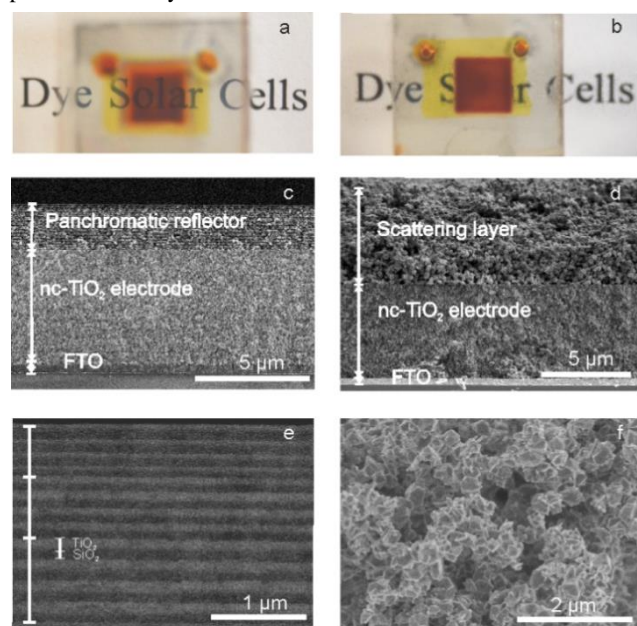
photonic multilayer.

Figure 1. Optical pictures of a) a cell in which a TiO$_2$–SiO$_2$ nanoparticle white light reflecting photonic multilayer has been integrated and b) a diffuse scattering TiO$_2$ layer based cell. The underlying text can only be
5 distinguished through the former. c) FESEM image of the cross-section of a nanocrystalline TiO$_2$ electrode onto which a white reflecting multilayer has been deposited and, e), its magnified view attained by backscattered electron detection, which allows to distinguish the three different periodicities. d) FESEM image of a diffuse scattering layer coupled to a
10 TiO$_2$ electrode and, f), its magnified view.

Field emission scanning electron microscopy (FESEM) images corresponding to cross-sections of a TiO$_2$ nanocrystalline electrode coupled to a white-light reflecting photonic crystal and a diffuse scattering layer made from a standard commercial paste
15 are displayed in figure 1.c and figure 1.d, respectively. Please notice that the total thickness of the heterogeneous photonic crystal structure herein proposed is around 2 μm, which is significantly thinner than that of the typical diffuse scattering layer (around 4 μm). Analysis of backscattered electron images,
20 like that shown in figure 1.e, reveals the smooth interface between the two types of porous films that form the broad band dielectric mirror, the different thickness of the SiO$_2$ (dark) and TiO$_2$ (bright) layers being readily appreciated. The polyhedral morphology of the particles in the diffuse scattering layer is
25 displayed in figure 1.f.

Total reflectance spectra measured for both the multilayered structures and the diffuse scattering layer after being coupled to the TiO$_2$ electrode are plotted in figure 2.a. In all cases, samples are infiltrated with ethanol (n=1.37) to approximate the actual
30 DSC operation conditions, in which the liquid electrolyte is filling the pores of the whole ensemble. The latter effect gives rise to lower reflected intensities as the dielectric contrast is decreased and, in the case of the multi-layered stacks, to a red-shift of the Bragg reflectance peak position. Such peak
35 displacement was taken into account when designing both the single and triple period photonic lattices to be integrated in the cells. Since photons are reflected by the diffuse scattering layer with a broad angular distribution, spectra were collected in all

cases using an integrating sphere. For the case of the photonic
40 crystal structures, the measured total reflectance shows minimum deviations with respect to the specular one, which evidences their low density of imperfections. The single periodicity structure (dashed line) presents a well-defined Bragg peak in the green region of the spectrum (λmax=530 nm), whereas the second one
45 yields a broader reflectance bandwidth (solid line) like the one displayed by the standard TiO$_2$ scattering layer (dashed-dotted line). In figure 2.b, ballistic transmittance spectra for the 1DPC based solar cells are plotted (dashed and solid lines for single and triple period structures, respectively), together with the spectra
50 obtained from a reference cell with the same electrode thickness both bare (short dashed line) and coupled to the diffuse scattering layer (dashed dotted line). It should be remarked that, while the multilayer based cells present an optical transmittance window at the longest visible wavelengths, the diffuse scattering layer turns
55 the cell opaque due to the lack of spectral selectivity of random light scattering. Device transparency data (ISO 9050:2003 standard) are collated in table 1. It can be observed that the semitransparency of DSCs decreases from around 25% down to 1% when diffuse scattering layers are employed. However, after
60 coupling single and triple period multilayers, transparency values close to 10% are obtained. In the case of the samples chosen as example, the transparency of the triple period multilayer is even higher than that of the single period 1DPC, which is a consequence of the high sensitivity of this parameter to small
65 changes around wavelengths for which the photopic response of the eye peaks, as explained in the supporting information (Please see supplementary figure S5).
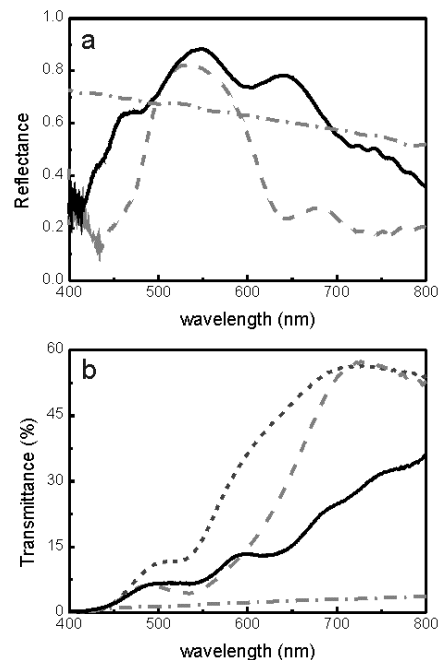

Figure 2. a) Total reflectance spectra of the optical multilayers (grey
70 dashed and black solid lines for the single and triple period structure, respectively) and the diffuse scattering layer (grey dashed-dotted line) coupled to the TiO$_2$ electrodes. b) Ballistic transmittance spectra from a reference DSC (dark grey short dashed line) and for those integrating a diffuse scattering layer (grey dashed-dotted line), a single periodicity
75 multilayer (grey dashed line) and a triple periodicity multilayer (black solid line).
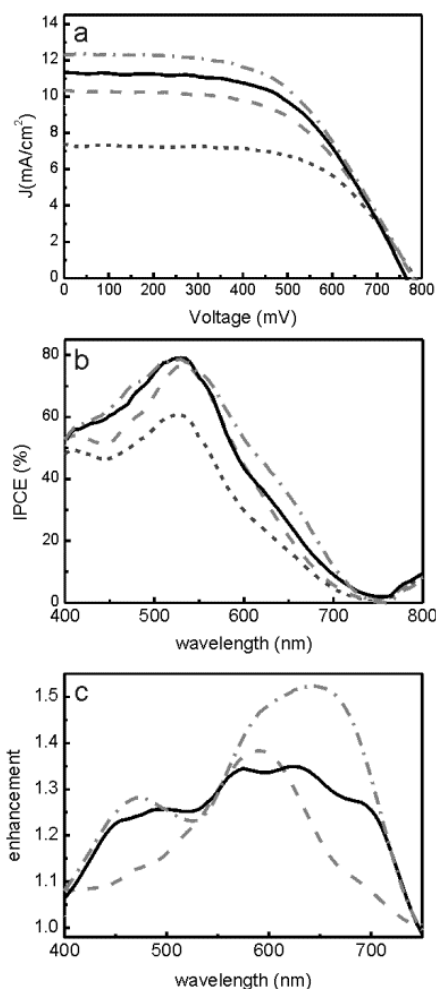
Figure 3. a) IV curves and b) incident photon to collected electron (IPCE) efficiencies measured from a reference cell (dark grey short dashed line) and cells integrating a diffuse scattering layer (grey dashed-dotted line) and two photonic crystal multilayers (grey dashed and black solid line for the single and triple period structures, respectively). c) IPCE enhancement factors obtained for the different cells (same line type and colour code).

Photocurrent–voltage (IV) curves were measured for the whole set of samples under standard AM1.5 illumination conditions of 100 mW/cm2 and are shown in figure 3.a. The main device parameters are presented in table 1. Comparatively, the multilayer based DSCs shows better photovoltaic performance than the reference and, among them, the panchromatic dielectric mirrors gives rise to higher short circuit photocurrent density (J_{sc}), as expected from its broader reflection band. By comparing the power conversion efficiency, η, calculated for these cells, one can see that the efficiency obtained from the white light reflecting PC based cell (4.9 %) is very similar to the value attained for the scattering-based cell (5.2 %). In the former case, this implies an enhancement in the efficiency of 40% with respect to the reference cell, which is the highest enhancement achieved by coupling a non-disordered porous back reflector to a standard thickness electrode. The fact that reflections arising from a random packing of large particles are oblique give rise to an extra enlargement of the optical path and thus of the probability of

absorption with respect to those achieved with a specular reflector, which explains the stronger reinforcement of efficiency observed for the diffusor. Also, spectral features of the cell performance were analysed by measuring the incident photon to current efficiency (IPCE) in all cases. Results are displayed in figure 3.b. The corresponding IPCE enhancement factors, γ, calculated as the ratio between the IPCE of the cells under study and that of the reference cell, are plotted in figure 3.c. The spectral region at which photocurrent generation is improved coincides, as expected, with those at which reflectance is maximum for each type of mirror integrated in the cell. As it can be seen, both the white light reflecting multilayer based cell and the diffuse scattering based cell present similar profiles, covering the entire visible region, which is consistent with the observation of comparable conversion efficiencies from both devices.
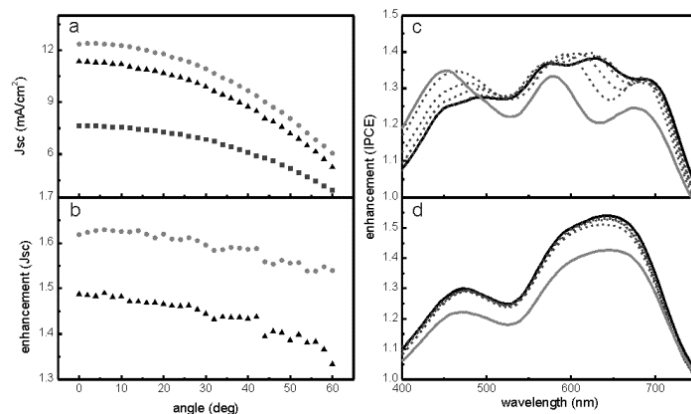

Figure 4. Angular dependence of photovoltaic parameters. a) Angular variation of the short circuit photocurrent density (Jsc) for the reference cell (dark grey squares) and cells integrating a white light reflecting multilayer (black triangles) and a diffuse scattering layer based cell (grey circles). b) Jsc enhancement attained for the different cells (same symbol and colour code). IPCE enhancement at different tilt angles for cells integrating, c), a white light reflecting multilayer and, d), a diffuse scattering layer, from θ=0 (black solid line) to θ=50 degrees (grey solid line).

In multilayers, light reflection results from interferometric effects and therefore its intensity and spectral features are dependent on the direction of propagation of light. It has been proved that the angular response of the photocurrent measured for 1DPC based DSCs shows deviations with respect to that of a standard semitransparent cell,[16] which follows Lambert's cosine law resulting from the decrease of the effective cross section or apparent surface of the device as it is inclined with respect to a collimated beam. In order to analyse these effects, both IV and IPCE curves were collected at different illumination angles for all cells. In figure 4.a we plot the angular variation of the Jsc measured at 1 sun for the white reflecting multilayer and the diffuse scattering based cells. Results for the semitransparent standard reference cell are also included for the sake of comparison. All tilted cells present performance losses that follow, with minimum deviations, the expected cosine law (please see supporting information, supplementary figures S6 and S7, for a more detailed analysis). The corresponding evolution of the photocurrent enhancement factors is drawn in figure 4.b. This graph shows that, for a wide range of tilt angles, integration of a panchromatic dielectric mirror provides an improvement of light

Physical Chemistry Chemical Physics

harvesting almost as independent of the illumination direction as that achieved with the diffuse scattering layer. This effect is observed for light beams impinging between the normal to the cell and approximately 45°. Above that incidence angle, the blue-shift of the photonic crystals reflectance gives rise to lower enhancements at red light frequencies, as it is observed in the IPCE enhancement spectra of the triple period multilayer based cell shown in figure 4.c. This effect is not compensated by the better performance detected in the blue region and gives rise to a decrease of the overall enhancement with respect to that of the diffuse scattering layer. A similar analysis performed for the diffuse scattering based cell shows that, although the magnitude of the enhancement is also reduced, its relative spectral distribution remains unaltered as the cell is tilted, as it can be seen in figure 4.d.

Conclusion

The results herein presented demonstrate that, by integrating a white light reflecting photonic crystal into a dye solar cell it is possible to reach efficiency values similar to those attained with diffuse scattering-based cells, without the adverse effect the latter ones have on the cell transparency. This is achieved by depositing a nanoparticle based one dimensional photonic crystal heterostructure with multiple periodicities on top of the nanocrystalline titania electrode. This advance was possible due to the strict control over the overall porosity and pore size distribution of the photonic crystal constituent layers. Integration of panchromatic specular reflectors of optimized diffusion in DSC means a step forwards towards highly efficient photovoltaic window modules for building integrated photovoltaics based on this third generation technology. Panchromatic mirrors could be designed to match the absorption of any dye attached to the mesoporous titania electrode, so they can be adapted easily to enhance the performance of a cell that provides the desired color in transmission. This type of mirror could also be useful for tandem cells, in which only well-defined ranges of light should be back reflected at different depths of the module.

Optical back scattering material	Transparency (%)	J_{sc} (mA/cm^2)	Voc (mV)	FF (%)	η (%)
None (reference cell)	24	7.33±0.3	786±8	60.3±3.2	3.5±0.2
single periodicity multilayer	8.7	10.34±0.3	780±16	55.3±1.8	4.5±0.2
Triple periodicity multilayer	9.5	11.35±0.4	765±14	56.1±3.4	4.9±0.4
Diffusor	1	12.35±0.8	780±20	54.1±2.7	5.2±0.4

Table 1. Values attained for transparency, short circuit photocurrent density (Jsc), open circuit photovoltage (Voc), fill factor (ff), and power conversion efficiency (η) for the different optical back scattering materials tested.

Acknowledgements

Notes and references

*Multifunctional Optical Materials Group, Instituto de Ciencia de Materiales de Sevilla, Consejo Superior de Investigaciones Científicas-Universidad de Sevilla (US-CSIC), Américo Vespucio 49, 41092 Sevilla, Spain. *E-mail: h.miguez@csic.es*

[1] S. Ito, S.M. Zakeeruddin, R. Humphry-Baker, P. Liska, R. Charvet, P. Comte, M.K. Nazeeruddin, P. Péchy, M. Takata, H. Miura, S. Uchida, M. Grätzel, *Adv.Mater.* 2006, **18**, 1202.

[2] Y. Chiba, A. Islam, Y. Watanabe, R. Komiya, N. Koide, L. Han, *Jpn. J.Appl. Phys.*, 2006, **45**, 25.

[3] C. Chen, M. Wang, J. Li, N. Pootrakulchote, L. Alibabaei, C. Ngoc-le, JD. Decoppet, J.Tsai, C. Grätzel, C.Wu, SM. Zakeeruddin, M. Grätzel, *ACS Nano*, 2009, **3**, 3103.

[4] Y. Cao, Y. Bai, Q. Yu, Y. Cheng, S. Liu, D. Shi, F. Gao, P. Wang, J Phys Chem C, 2009, **113**, 6290.

[5] A. Yella, H. W. Lee, H. N. Tsao, C. Yi, A. K. Chandiran, M. K. Nazeeruddin, E. W. G. Diau, C. Y. Yeh, S. M. Zakeeruddin, and M. Grätzel, *Science*, 2011, **334**, 629.

[6] S.Nishimura, N.Abrams, B. A. Lewis, L. I. Halaoui, T. E. Mallouk, K. D. Benkstein, J. van de Lagemaat, A.J. Frank, *J. Am. Chem. Soc.*, 2003, **125**, 6306.

[7] S. Colodrero, A. Mihi, L. Häggman, M. Ocaña, G. Boschloo, A. Hagfeldt and H. Míguez, *Adv. Mater.*, 2009, **21**, 764.

Physical Chemistry Chemical Physics Accepted Manuscript

8 S. Guldin, S. Huttner, M. Kolle, M.E. Welland, P. Müller-Buschbaum, R.H. Friend, N. Steiner, N. Tetreault., *Nano Lett.*, 2010, **10**, 2303.

9 C.T. Yip, H. Huang, L. Zhou, K. Xie, Y. Wang, T. Fenq, J. Li. W.Y. Tam, *Adv.Mater*., 2011, **23**, 5624.

10 D. Colonna, S. Colodrero, H. Lindström, A. Di Carlo, H. Míguez, *Energy Environ. Sci.* 2012, **5**, 8238.

11 M. Guo, K.Y. Xie, J. Lin, Z.H. Yong, C.T. Yip, L.M. Zhuo, Y. Wang, H.T. Huang, *Energy Environ. Sci.* 2012, **5**, 9881.

12 S. Colodrero, A. Forneli, C. López-López, L. Pellejà, H. Míguez, E. Palomares, *Adv. Funct. Mater*. 2012, **22**, 1303.

13 C. López-López, S. Colodrero, S. R. Raga, H. Lindström, F. Fabregat-Santiago, J. Bisquert, H. Míguez, *J. Mater. Chem*., 2012, **22**, 1751.

14 S.D. Burnside, V. Shklover, C. Barbe, P. Comte, F. Arendse, K. Brooks, M. Grätzel, *Chem. Mater*., 1998, **10**, 2419.

15 G. Lozano, S. Colodrero, O. Caulier, M.E. Calvo, H. Míguez, *J. Phys. Chem. C* 2010, **114**, 3681.

16 C. López-López, S. Colodrero, ME. Calvo, H. Míguez, *Energy Environ. Sci.*, 2013, **6**, 1260.